Analytical expansion of highly focused vector beams into vector spherical harmonics and its application to Mie scattering

S. Orlov,[1,2,*] U. Peschel,[2,3] T. Bauer,[1,2] and P. Banzer[1,2,3]
[1]*Max Planck Institute for the Science of Light, D-91058, Erlangen, Germany*
[2]*Institute of Optics, Information and Photonics, University of Erlangen-Nuremberg, D-91058, Erlangen, Germany*
[3]*Cluster of Excellence "Engineering of Advanced Materials" (EAM), University of Erlangen-Nuremberg, D-91052, Erlangen, Germany*
(Received 17 April 2012; published 22 June 2012)

The analytical expansion of linearly, azimuthally, and radially polarized rigorous beam-type solutions of Maxwell's equations into vector spherical harmonics (VSHs) is presented. We report on the dominance of higher order multipoles in highly focused radially and azimuthally polarized beams compared to linearly polarized beams under similar conditions. Furthermore, we theoretically investigate a scenario in which highly focused azimuthally and radially polarized beams interact with a linear polarizer placed in the focal plane and expand the resulting fields into VSHs. The generalized Mie theory is used afterwards to investigate the scattering of the studied beams off a spherical gold nanoparticle.

DOI: 10.1103/PhysRevA.85.063825 PACS number(s): 42.25.Bs, 42.25.Fx, 42.25.Ja, 42.79.Ci

I. INTRODUCTION

During the last decade, numerous works have been undertaken to characterize, elaborate, and manipulate single nanoscaled objects. Metal nanoparticles are among the hot topics of active research in nanoscience [1] and related branches such as nanobiology [2], nano-optics [3], nanophotonics, and nanoplasmonics [4,5]. Single nanoparticles are the building blocks of complex nanostructures [6], and their relative arrangement [7] strongly influences the collective response of plasmonic nanoparticle aggregates [8,9].

The theoretical description of light-particle interaction started from the classical theory of a linearly polarized plane wave scattering off a sphere [10] and was extended after the invention of the laser. The first studies on how a spherical particle illuminated by a Gaussian beam responds to the incident field have revealed deviations from the classical theory [11,12]. Thereafter, numerous works devoted to modeling the optical response of homogeneous spheres illuminated with Gaussian beams, described by a complex source model [13] or in the framework of the Bromwich formalism [14], have been reported along with other studies [15]. In contrast to the use of a Gaussian beam, the recently renowned interest in highly focused optical beams is mainly concerned with the polarization state of the beam, which strongly influences the size and shape of the focal spot [16]. In particular, the role of azimuthal and radial polarization has been investigated both theoretically [17] and experimentally [18]. In recent publications the interaction between highly focused beams and nanoparticles has been investigated [4,19–21]. These works have clearly demonstrated that the optical response is strongly dependent on both the particle location relative to the beam focus and the polarization structure of the beam and differs notably from that of plane wave illumination.

To describe these highly focused beams theoretically, one can start from the exact analytical solution of the scalar wave equation by the complex source beam (CSB) [22]. This can be extended toward a full solution of Maxwell's equations, which accurately describes highly focused linearly, radially, and azimuthally polarized light beams [23].

The aim of this paper is to investigate an analytical expansion of the vector CSBs [23] into VSHs, i.e., electromagnetic multipoles [24]. Such an expansion is essential to understand the interaction of light fields with nano-objects such as atoms, molecules, or particles, which are all of subwavelength dimensions. Those nano-objects locally sense only the various multipole components of the incident field [25]. The dipole components as the first order of the expansion are the most important ones, but even objects such as (meta-) atoms already respond to quadrupole and even higher order excitations [26,27]. Having found the expansion into multipoles it is, for example, straightforward to describe the interaction of a beam with a spherical particle as is done in classical Mie theory for a plane wave excitation. The expansion into VSHs also allows for an analysis of the interaction of focused beams with larger objects, which are conveniently described by a T matrix, the basis functions of which are again VSHs [28,29]. Moreover, the multipole approach provides a simple measure of the purity of the longitudinal field mode and is efficient for calculating the field in the focal region of a lens [30].

In the first section we start with a brief introduction to the expressions of vector CSBs. In the next section we develop an analytical expansion of the CSBs into VSHs. Finally, we use the generalized Mie theory to investigate the scattering problem for a nanoparticle illuminated by CSBs. In particular, we reveal that the interaction of a radially polarized beam with a particle is stronger than that of a linearly polarized one.

II. EXPANSION OF HIGHLY FOCUSED VECTOR BEAMS INTO VSHs

A. Expansion of the scalar complex source beam

To generate vectorial CSB solutions we start from the scalar one [22], which is defined as

$$\begin{Bmatrix} \mathrm{Rg}\, u(\mathbf{r}) \\ u(\mathbf{r}) \end{Bmatrix} = U_0 \begin{Bmatrix} j_0(ks) \\ i h_0^{(1)}(ks) \end{Bmatrix}, \quad k = \frac{\omega}{c}, \tag{1}$$

*Sergejus.Orlovas@mpl.mpg.de

where j_0 and h_0 are spherical Bessel functions of first and third kind, namely, $j_0(x) = \sin(x)/x$ and $h_0(x) = \exp(ix)/x$. Here the first line corresponds to the regular solution (suffix "Rg") and the second line to the irregular one. U_0 is a normalization constant. The complex distance s is defined as $s(\mathbf{r}) = [x^2 + y^2 + (z - iz_0)^2]^{1/2}$ in Cartesian, or as $s(\mathbf{r}) = [r^2 - 2irz_0\cos\theta - z_0^2]^{1/2}$ in spherical coordinates $[\mathbf{r} = (r,\theta,\phi)]$. The Rayleigh distance z_0 is related to the waist of the beam w_0 as $z_0 = kw_0^2/2$. Further, we make the "beam" choice for a branch cut $(\mathrm{Im}[s(\mathbf{r})] \leqslant 0)$ [22,23]. It guarantees a constant power flow in forward direction, where the irregular solution also includes a ring of sources at $x^2 + y^2 = z_0^2$ (for a more detailed discussion of the different solutions see Ref. [23]). The normalization constant U_0 is thus

$$U_0 = g_0^{-1}(ikz_0) = \begin{cases} U_r = kz_0/\sinh(kz_0), \\ U_i = kz_0\exp(kz_0), \end{cases} \tag{2}$$

where g_0 is a short notation of a either regular (r) or irregular (i) spherical Bessel function.

To generate a system of basis functions which we can use to represent the CSB we start from the eigenfunctions of the scalar wave equation in spherical coordinates (scalar multipoles), which are expressed as [24]

$$u_{mn}(\mathbf{r}) = g_n(kr)P_n^m(\cos\theta)\exp(im\phi), \tag{3}$$

where P_n^m is the associated Legendre polynomial, which we define as in Ref. [28], and m, n are integer numbers. Here g_n is either a regular (nonsingular) spherical Bessel function of the first kind j_n or an irregular (singular) function of the third kind $h_n^{(1)}$.

Our intention is to expand the scalar CSB (1) into scalar multipoles. This expansion is formally given by

$$u(\mathbf{r}) = \sum_{n=0}^{\infty} a_n u_{0n}(\mathbf{r}), \tag{4}$$

where only radially symmetric basis functions have to be taken into account. The decomposition coefficients in the source-free region are determined from the integral

$$a_n = \frac{2n+1}{2g_n(kr_d)} \int_0^{\pi} u(r_d,\theta)P_n(\cos\theta)\sin\theta\, d\theta, \tag{5}$$

where r_d is the distance from the waist of the beam (for the irregular solution $r_d \leqslant z_0$). Next, we employ the addition theorem for spherical Bessel functions, and after redefining it for complex values we readily obtain the expansion coefficients $a_n^{(i)}$ of an irregular solution as

$$a_n^{(i)} = kz_0(2n+1)\exp(-kz_0) \begin{cases} j_n(kz_0 i), & \text{if } r_d \leqslant z_0, \\ h_n^{(2)}(kz_0 i), & \text{if } r_d \geqslant z_0. \end{cases} \tag{6}$$

In the case of infinite width $(z_0 \to \infty)$ the expansion coefficients $a_n^{(i)}$ converge to those of a plane wave $a_n^{\text{plane}} = i^n(2n+1)$, due to our choice of the normalization constant U_0; see (2).

For a regular solution, the expansion coefficients $a_n^{(r)}$ are slightly different:

$$a_n^{(r)} = kz_0 \frac{(2n+1)}{\sinh(kz_0)} j_n(kz_0 i). \tag{7}$$

From here on we will mainly consider the regular solution $u(r)$, and the irregular solution will be briefly discussed throughout the paper when necessary.

B. Expansion of radially and azimuthally polarized beams

The azimuthally $\mathbf{U}_M$ and radially $\mathbf{U}_N$ polarized vector complex source beams are defined as in Ref. [23] and can be expressed as

$$\mathbf{U}_M(\mathbf{r}) = \nabla u(\mathbf{r}) \times \mathbf{r}, \quad \mathbf{U}_N(\mathbf{r}) = \frac{1}{k}\nabla \times \mathbf{U}_M(\mathbf{r}). \tag{8}$$

The function $\mathbf{U}_M$ has only azimuthal components, so it represents the electric field $\mathbf{E}_M = E_0\mathbf{U}_M$ of an azimuthally polarized highly focused CSB, where E_0 is an amplitude. The function $\mathbf{U}_N$ represents the electric field $\mathbf{E}_N = E_0\mathbf{U}_N$ of a radially polarized CSB. The magnetic fields $\mathbf{H}$ of both beams can be generated using $i\omega\mu_0\mathbf{H} = \nabla \times \mathbf{E}$. It turns out that the vector function $\mathbf{U}_N$ also describes the magnetic field $\mathbf{H}_N = H_0\mathbf{U}_N$ of an azimuthally polarized beam $E_0\mathbf{U}_M$ and $\mathbf{U}_M$ that of a radially polarized one [23].

The family of the orthogonal VSHs $\mathbf{M}_{mn}$, $\mathbf{N}_{mn}$ [24] is obtained from the scalar spherical multipoles (3) after applying the same operators as in Eq. (8). The substitution of the sum (4) into Eq. (8) results in the following expansions of radially and azimuthally polarized beams into VSHs, which we write as

$$\mathbf{U}_M = \sum_{n=1}^{\infty} A_n \widetilde{\mathbf{M}}_{0n}, \quad \mathbf{U}_N = \sum_{n=1}^{\infty} A_n \widetilde{\mathbf{N}}_{0n}, \tag{9}$$

where $\widetilde{\mathbf{M}}_{0n} = \gamma_{0n}\mathbf{M}_{0n}$ and $\widetilde{\mathbf{N}}_{0n} = \gamma_{0n}\mathbf{N}_{0n}$ are normalized VSHs [28]. The γ_{mn} are the standard normalization constants (see Ref. [28]), and the normalized expansion coefficients thus are $A_n = a_n/\gamma_{0n}$.

The dependence of the expansion coefficients A_n on the collimation distance kz_0 and the multipole order n is shown in Fig. 1. Here we note that the differences in the expansion coefficients between regular and irregular complex source beams appear only at values of the collimation distance $kz_0 < n$. The natural cause for this divergent behavior is the presence of virtual sources in the irregular beam [23].

C. Interaction of radially and azimuthally polarized beams with a linear polarizer and expansion of resulting fields into VSHs

Radially, azimuthally and linearly polarized beams are most commonly used in scattering problems. However, more complicated polarization states (highly focused linearly polarized TEM_{01} and TEM_{10} modes) for investigation of nanostructures received attention just recently [4]. Therefore, in this section we consider such linearly polarized TEM_{01} and TEM_{10} modes under tight focusing conditions to address the growing interest in these more complicated field structures. These modes can be usually achieved by transmitting paraxially propagating radially or azimuthally polarized beams through a linear polarizer.

In what follows, we will investigate a theoretical scenario in which a linear polarizer is placed in the focal plane of the highly focused radially and azimuthally polarized CSBs, which we discussed already before. We investigate how the linear polarizer transforms the expansion coefficients of arbitrary incident fields. We also briefly interpret the resulting beam

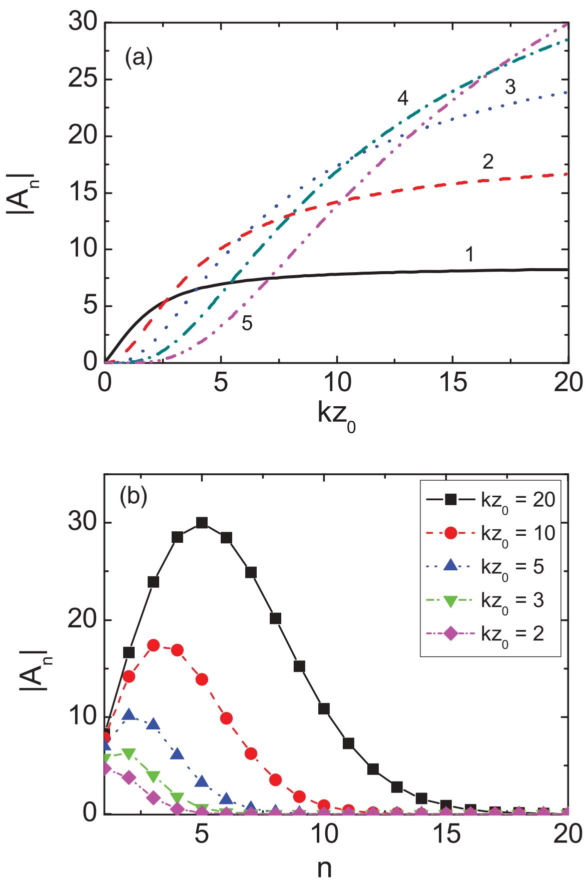

FIG. 1. (Color online) (a) Dependence of the different expansion coefficients $|A_n|$ on the collimation distance kz_0 for regular and irregular solutions. The multipole order n is shown. (b) Dependence of the different expansion coefficients $|A_n|$ on the multipole order for regular solutions for different kz_0.

configurations and attribute them to possible experimental realizations.

Therefore, we need to define the action of a polarizer which is placed in a nonparaxial beam. In this context, the theoretical description of paraxial polarizers is well established [31]. However, insights into the theory of nonparaxial polarizers are only emerging [32]; thus we define a linear polarizer as follows: We assume that a linear polarizer acts only on the electric field of the beams (8) and require that the plane wave spectrum remains transverse, so the resulting spectrum can be written as

$$\mathbf{U}_M^{p_x} \to (\mathbf{U}_M\cdot\mathbf{p}_x)\mathbf{p}_x,\quad \mathbf{U}_N^{p_x} \to (\mathbf{U}_N\cdot\mathbf{p}_x)\mathbf{p}_x, \tag{10}$$

where $\mathbf{p}_x = \mathbf{e}_x - \mathbf{e}_r(\mathbf{e}_x\cdot\mathbf{e}_r)$ and $\mathbf{e}_x = \mathbf{e}_r\sin\theta\cos\phi + \mathbf{e}_\theta\cos\theta\cos\phi - \mathbf{e}_\phi\sin\phi$ is a unit vector oriented along the x axis. We note that contrary to the definition of Ref. [32] the nonparaxial polarizer model used here [Eq. (10)] mimics an experimentally realizable situation, when the transmission decreases with increasing angles of incidence. Another pair of beams $\mathbf{U}_M^{p_y}$, $\mathbf{U}_N^{p_y}$ is obtained by interchanging $\mathbf{e}_x$ in Eq. (10) with $\mathbf{e}_y$. In this manner we end up with four beam configurations. A curl of each beam provides us with further four TEM-like beam configurations, $\mathbf{U}_M^{\pi_x}$, $\mathbf{U}_M^{\pi_y}$, $\mathbf{U}_N^{\pi_x}$, and $\mathbf{U}_N^{\pi_y}$. In general, $\mathbf{U}_N^{\pi_x} \neq (ik)^{-1}\nabla\times\mathbf{U}_M^{p_y}$, and thus the last four beams represent different configurations of a linear polarizer.

Upon substitution of Eq. (9) into Eq. (10), the beam expansion reduces to the decomposition of the vector functions $(\mathbf{M}_{0n}\cdot\mathbf{p}_x)\mathbf{p}_x$ and $(\mathbf{N}_{0n}\cdot\mathbf{p}_x)\mathbf{p}_x$ into VSHs. After rather tedious analytical calculations we arrive at the following expression for the term $(\mathbf{M}_{0n}\cdot\mathbf{p}_x)\mathbf{p}_x$:

$$\begin{aligned}(\mathbf{M}_{0n}\cdot\mathbf{p}_x)\mathbf{p}_x &= \sum_{\nu=1}^{\infty}\delta_{\nu,n}\left[\frac{\mathbf{M}_{0\nu}}{2}+\frac{\mathbf{M}_{2\nu}}{4\nu(\nu+1)}+\frac{\mathbf{M}_{-2\nu}(\nu-1)(\nu+2)}{4}\right]\\ &\quad +\frac{i}{4}\left[\frac{\delta_{\nu,n+1}}{\nu(2\nu-1)}-\frac{\delta_{\nu,n-1}}{(\nu+1)(2\nu+3)}\right]\left[\mathbf{N}_{2\nu}-\frac{(\nu+2)!}{(\nu-2)!}\mathbf{N}_{-2\nu}\right].\end{aligned} \tag{11}$$

We see that for $n = 1$ a magnetic dipole $\mathbf{M}_{01}$ is present, and its amplitude is half of the initial dipole. Thus, the nonparaxial polarizer absorbs half of the energy of the dipole. A curl of (11) produces an electric dipole $\mathbf{N}_{01}$, whose dipole moment is oriented in the z direction. We note also an appearance of magnetic and electric multipoles with $m = \pm 2$. The expansion of $(\mathbf{N}_{0n}\cdot\mathbf{p}_x)\mathbf{p}_x$ is written as

$$\begin{aligned}(\mathbf{N}_{0n}\cdot\mathbf{p}_x)\mathbf{p}_x = \sum_{\nu=1}^{\infty}\frac{\mathbf{N}_{0\nu}}{2}&\left[\delta_{\nu,n}\frac{2\nu^2+2\nu-3}{(2\nu-1)(2\nu+3)}-\delta_{\nu,n+2}\frac{(\nu-1)(\nu-2)}{(2\nu-3)(2\nu-1)}-\delta_{\nu,n-2}\frac{(\nu+3)(\nu+2)}{(2\nu+3)(2\nu+5)}\right]\\ &+\frac{1}{4\nu(\nu+1)}\left\{i\left[\frac{(\nu+2)\delta_{\nu,n-1}}{(2\nu+3)}-\frac{(\nu-1)\delta_{\nu,n+1}}{(2\nu-1)}\right]\left[\mathbf{M}_{2\nu}-\frac{(\nu+2)!}{(\nu-2)!}\mathbf{M}_{-2\nu}\right]\right.\\ &\left.-\left[\frac{(2\nu^2+2\nu+3)\delta_{\nu,n}}{(2\nu-1)(2\nu+3)}-\frac{\delta_{\nu,n+2}(\nu+1)(\nu-2)}{(2\nu-3)(2\nu-1)}-\frac{\delta_{\nu,n-2}\nu(\nu+3)}{(2\nu+3)(2\nu+5)}\right]\left[\mathbf{N}_{2\nu}+\frac{(\nu+2)!}{(\nu-2)!}\mathbf{N}_{-2\nu}\right]\right\}.\end{aligned} \tag{12}$$

A particularly interesting result is that for $n = 1$ the electric dipole $\mathbf{N}_{01}$ field has $1/10$ of the amplitude of that before passing through a linear polarizer, and a sextupole $\mathbf{N}_{03}$ appears in the expansion to compensate the remaining longitudinal electric field component. Thus, the operation of the nonparaxial polarizer results in a decreased dipole moment of the beam and an effective defocusing of the resulting beam [30]; see Fig. 2.

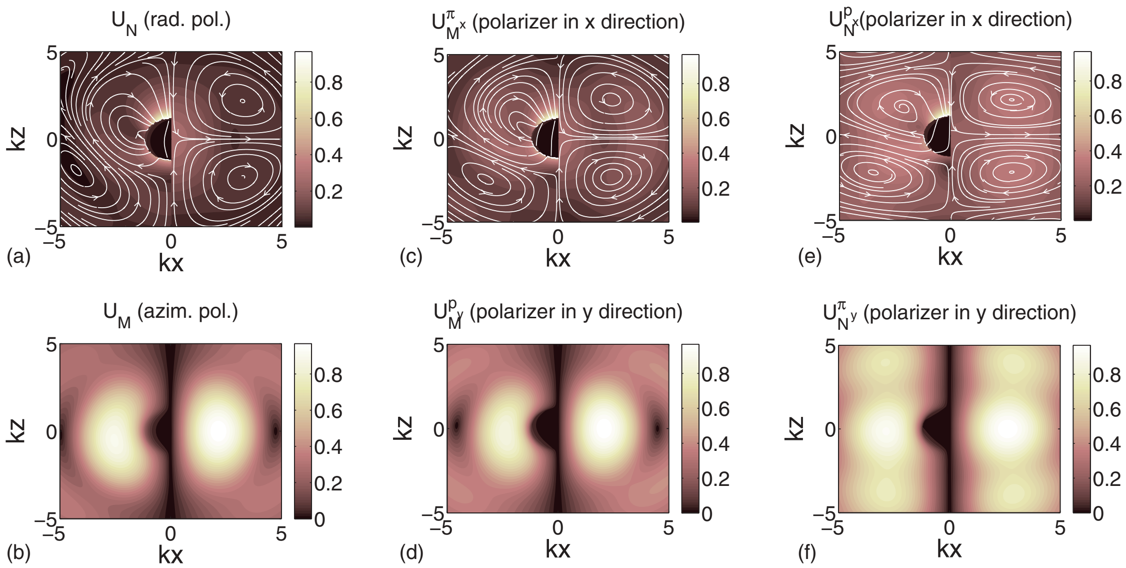

FIG. 2. (Color online) Modulus of the total (left side) and incident (right side) fields for radially (a) and azimuthally (b) polarized CSB scattered off a gold sphere. Corresponding distributions for CSBs interacting with a linear polarizer and scattered off a gold sphere (c)–(f). The radius of the sphere is $R_{sp} = 75$ nm, the wavelength is $\lambda = 780$ nm, and $kz_0 = 1.5$. The white arrows (a, c, e) depict the direction of the electric field $\mathbf{E}$. The arrows are not shown in panels b, d, and f.

The decompositions (11) and (12) contain terms with $m = 0$ and $m = \pm 2$, so the linearly polarized beams $\mathbf{U}_M^{p_x}$ and $\mathbf{U}_N^{p_x}$ are expressed by the corresponding sums

$$\mathbf{U}_M^{p_x} = \sum_{n=1}^{\infty} A_{0n}^M \widetilde{\mathbf{M}}_{0n} + \left[A_{2n}^M(\widetilde{\mathbf{M}}_{2n} + \widetilde{\mathbf{M}}_{-2n}) + B_{2n}^M(\widetilde{\mathbf{N}}_{2n} - \widetilde{\mathbf{N}}_{-2n})\right],$$
$$\mathbf{U}_N^{p_x} = \sum_{n=1}^{\infty} B_{0n}^N \widetilde{\mathbf{N}}_{0n} + \left[B_{2n}^N(\widetilde{\mathbf{N}}_{2n} + \widetilde{\mathbf{N}}_{-2n}) + A_{2n}^N(\widetilde{\mathbf{M}}_{2n} - \widetilde{\mathbf{M}}_{-2n})\right], \tag{13}$$

where

$$\gamma_{0n} A_{0n}^M = \frac{a_n}{2}, \quad \gamma_{2n} A_{2n}^M = \frac{a_n}{4n(n+1)},$$
$$\gamma_{2n} A_{2n}^N = -U_0 i \frac{(n-1)g_{n-1}^* - (n+2)g_{n+1}^*}{4n(n+1)} \tag{14}$$

and

$$\gamma_{0n} B_{0n}^N = \frac{U_0}{2}\left[\frac{(2n+1)(2n^2+2n-3)g_n^*}{(2n-1)(2n+3)} - \frac{(n-1)(n-2)g_{n-2}^*}{(2n-1)} - \frac{(n+2)(n+3)g_{n+2}^*}{(2n+3)}\right],$$
$$\gamma_{2n} B_{2n}^N = -\frac{U_0}{4n(n+1)}\left[\frac{(2n+1)(2n^2+2n+3)g_n^*}{(2n-1)(2n+3)} - \frac{(n+1)(n-2)g_{n-2}^*}{(2n-1)} - \frac{n(n+3)g_{n+2}^*}{(2n+3)}\right],$$
$$\gamma_{2n} B_{2n}^M = U_0 i \frac{(n+1)g_{n-1}^* - n g_{n+1}^*}{4n(n+1)}. \tag{15}$$

Here g_n^* denotes either j_n or $h_n^{(2)}$. The most intriguing feature of the linearly polarized $\mathbf{U}_M^{p_x}$ beam is the absence of the electric dipole and the presence of relatively strong electric quadrupoles in the expansion of the beam (13). Thus, this configuration may be a promising tool in the studies of quadrupole responses of various scatterers.

In the limit of large beam widths $kz_0 \to \infty$, we have $g_n^* = i^n/U_0$, and expressions (14, 15) are simplified to

$$\gamma_{0n} A_{0n}^M = \gamma_{0n} B_{0n}^N = \frac{(2n+1)i^n}{2},$$
$$\gamma_{2n} A_{2n}^M = -\gamma_{2n} A_{2n}^N = \frac{(2n+1)i^n}{4n(n+1)},$$
$$\gamma_{2n} B_{2n}^M = -\gamma_{2n} B_{2n}^N = \frac{(2n+1)i^n}{4n(n+1)}; \tag{16}$$

thus, for $kz_0 \to \infty$ we have $\mathbf{U}_N^{\pi_x} = k^{-1}\nabla \times \mathbf{U}_M^{p_y}$. The typical dependencies of the expansion coefficients are presented in Fig. 3.

The natural question arises how the discussed beam configurations can be experimentally realized. In order to address this concern, we formally introduce the following theoretical scenario. The vectors $\mathbf{p}_x$ and $\mathbf{p}_y$ can be written in the small angle approximation ($\theta \approx 0$) as $\mathbf{p}_x^{(p)} = \mathbf{e}_\theta \cos\phi - \mathbf{e}_\phi \sin\phi$ and $\mathbf{p}_y^{(p)} = \mathbf{e}_\theta \sin\phi + \mathbf{e}_\phi \cos\phi$. We note that the θ components now do not depend on the angle of incidence. Upon passing through a focusing system with high numerical aperture the paraxial ($|E_z| \ll \sqrt{|E_\rho|^2 + |E_\phi|^2}$) vector field $\mathbf{E} = E_\rho \mathbf{e}_\rho + E_\phi \mathbf{e}_\phi$ at the entrance of the pupil of a focusing system is converted into a plane wave with an amplitude $\mathbf{E} \approx E_\rho \mathbf{e}_\theta + E_\phi \mathbf{e}_\phi$ after the output pupil. So, if a linear polarizer oriented in x direction is placed in front of the entrance pupil, the unitary vectors of a cylindrical coordinate system ($\mathbf{e}_\rho, \mathbf{e}_\phi$) are transformed into ($\mathbf{e}_\theta$, $\mathbf{e}_\phi$); thus the vector $\mathbf{e}_x = \mathbf{e}_\rho \cos\phi - \mathbf{e}_\phi \sin\phi$ is transformed into the vector $\mathbf{p}_x^{(p)}$. Furthermore, the repeating derivations of Eqs. (11) and (12) show the halved dipole amplitudes of $\mathbf{N}_{01}$ and $\mathbf{M}_{01}$ dipoles compared to the situation without a polarizer. Thus, the beam configurations $\mathbf{U}_N^{\pi_x}$, $\mathbf{U}_N^{\pi_y}$, $\mathbf{U}_M^{p_x}$, $\mathbf{U}_M^{p_y}$ can be attributed to the tightly focused TEM_{10} and TEM_{01} modes [4].

Next, we can backpropagate the action of the vectors $\mathbf{p}_x$, $\mathbf{p}_y$, thus revealing how the input field at the entrance has to

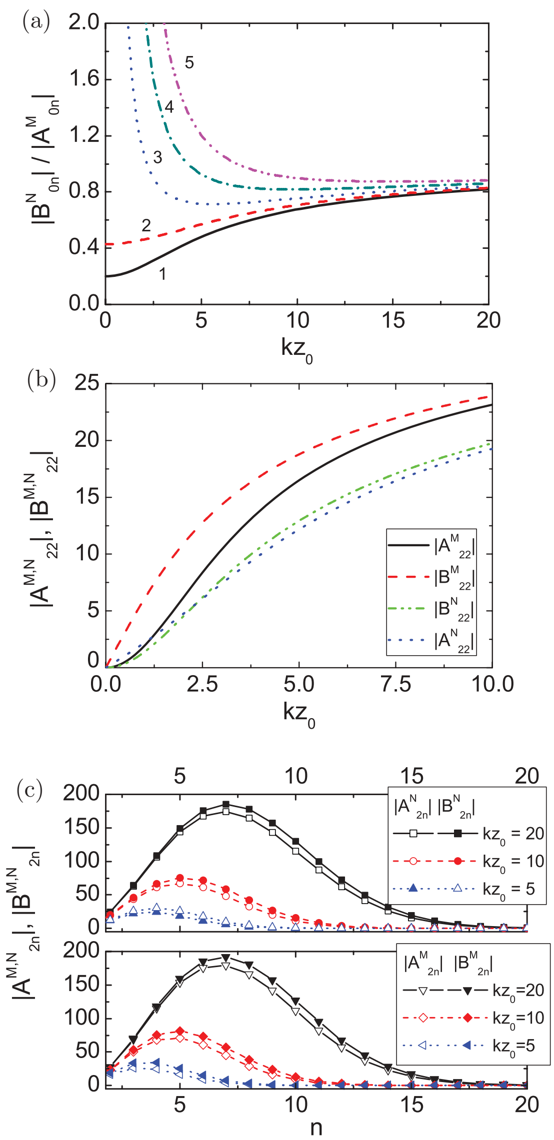

FIG. 3. (Color online) (a) Dependence of the ratio $|B^N_{0n}|/|A^M_{0n}|$ for CSBs interacting with a linear polarizer on the collimation distance kz_0. The multipole order n is shown. (b) Dependence of the expansion coefficients $|A^{M,N}_{22}|$ and $|B^{M,N}_{22}|$ of CSBs interacting with a linear polarizer on the collimation distance kz_0. (c) Dependence of the expansion coefficients $|A^{M,N}_{2n}|$ and $|B^{M,N}_{2n}|$ on the multipole order n.

be modified in order to realize $\mathbf{U}^{\pi_x}_M$, $\mathbf{U}^{\pi_y}_M$, $\mathbf{U}^{p_x}_N$, $\mathbf{U}^{p_y}_N$ beams. It turns out, that besides a linear polarizer an additional spatial modulation of the input field depending on the focusing system has to be performed.

D. Expansion of linearly polarized beams

We define electric fields of linearly polarized beams as [23]

$$\mathbf{U}^{(x)}_M(\mathbf{r}) = \nabla u(\mathbf{r})\times\frac{2\mathbf{e}_y}{k},\quad \mathbf{U}^{(y)}_N(\mathbf{r}) = \frac{1}{k}\nabla\times\mathbf{U}^{(x)}_M(\mathbf{r}),$$
$$\mathbf{U}^{(y)}_M(\mathbf{r}) = \nabla u(\mathbf{r})\times\frac{2\mathbf{e}_x}{k},\quad \mathbf{U}^{(x)}_N(\mathbf{r}) = \frac{1}{k}\nabla\times\mathbf{U}^{(y)}_M(\mathbf{r}), \tag{17}$$

so that in principle four beam choices are possible, see discussion in Ref. [23] for more details. We use the definition of the beams $\mathbf{U}^{(x)}_M$, $\mathbf{U}^{(y)}_N$ to expand the beams into VSHs. First, we decompose the vector function

$$\mathbf{L}_{0n}\times\frac{\mathbf{e}_y}{k} = \left[\mathbf{e}_r\frac{g_n(kr)}{kr}\frac{\partial}{\partial\theta}P_n(\cos\theta) + \mathbf{e}_\theta\frac{\partial g_n(kr)}{k\partial r}P_n(\cos\theta)\right]\cos\phi + \mathbf{e}_\phi\sin\phi\left[\frac{\partial g_n(kr)}{k\partial r}P_n(\cos\theta)\cos\theta - \frac{g_n(kr)}{kr}\frac{\partial}{\partial\theta}P_n(\cos\theta)\sin\theta\right], \tag{18}$$

where $\mathbf{L}_{0n}$ is a nonsolenoidal VSH [24]. For the sake of simplicity, we employ for the decomposition the fact that the functions $\mathbf{N}_{mn}$ have a nonzero radial component at the origin $r\to 0$. The decomposition into $\mathbf{M}_{mn}$ is performed on the other hand at infinity ($r\to\infty$). The complicated integration is omitted here, and the final expression is given as

$$\mathbf{L}_{0n}\times\frac{2\mathbf{e}_y}{k} = \sum_{\nu=1}^{\infty}\left[\frac{\mathbf{N}_{1,\nu}}{\nu(\nu+1)} - \mathbf{N}_{-1,\nu}\right]\delta_{\nu,n} + i\left[\frac{\mathbf{M}_{1,\nu}}{\nu(\nu+1)} + \mathbf{M}_{-1,\nu}\right] \times\left[\frac{\nu+1}{2\nu-1}\delta_{\nu,n+1} - \frac{\nu}{2\nu+3}\delta_{\nu,n-1}\right]. \tag{19}$$

The decomposition contains only terms with $m=\pm 1$, so the linearly polarized beam is expressed by the sum

$$\mathbf{U}^{(x)}_M = i\sum_{n=1}^{\infty}C_{1n}[\widetilde{\mathbf{M}}_{1n} + \widetilde{\mathbf{M}}_{-1n}] + D_{1n}[\widetilde{\mathbf{N}}_{1n} - \widetilde{\mathbf{N}}_{-1n}],$$
$$\mathbf{U}^{(y)}_N = i\sum_{n=1}^{\infty}C_{1n}[\widetilde{\mathbf{N}}_{1n} + \widetilde{\mathbf{N}}_{-1n}] + D_{1n}[\widetilde{\mathbf{M}}_{1n} - \widetilde{\mathbf{M}}_{-1n}], \tag{20}$$

where

$$\gamma_{1n}C_{1n} = U_0 i\left[\frac{g^*_{n-1}}{n} - \frac{g^*_{n+1}}{n+1}\right],\quad \gamma_{1n}D_{1n} = U_0\frac{(2n+1)\,g^*_n}{n\,(n+1)}, \tag{21}$$

and the complex conjugated g^*_n denotes either j_n or $h^{(2)}_n$. The coefficients for $m=1$ and $m=-1$ are closely related. It holds that $C_{1n} = C_{-1n}$ and $D_{1n} = -D_{-1n}$. The beams $\mathbf{U}^{(x)}_M$ and $\mathbf{U}^{(y)}_N$ are represented at the origin $\mathbf{r}=0$ by electric and magnetic dipoles whose moments are perpendicular to each other in the transverse plane. For example, the beam $\mathbf{U}^{(x)}_M$ (20) consists of a pair of two dipoles: An electric dipole oriented along the x direction, and a magnetic dipole along the y direction. For $z_0\to\infty$ the expansion coefficients C_{1n} and D_{1n} are equal and coincide with those of a plane wave. If $kz_0 = 0$, the coefficients D_{1n} are zero and the only nonzero expansion coefficients are $C_{\pm 11}$. Thus, for small z_0 the solution $\mathbf{U}^{(x)}_M$ represents the radiation of a magnetic dipole oriented along

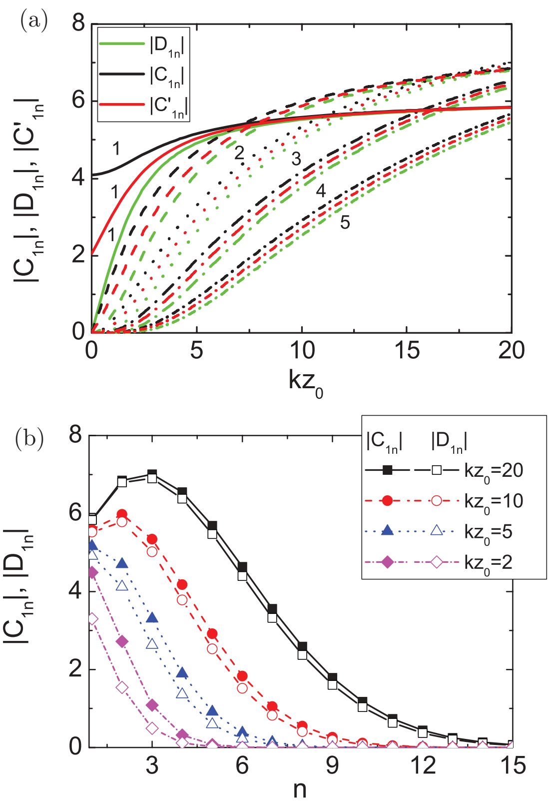

FIG. 4. (Color online) (a) Dependence of the first five ($n = 1,2,3,4,5$) expansion coefficients $|C_{1n}|$, $|D_{1n}|$, and $|C'_{1n}|$ for linearly polarized regular CSB on the collimation distance kz_0. (b) Dependence of the expansion coefficients $|C_{1n}|$ and $|D_{1n}|$ for linearly polarized regular CSBs on the multipole order.

y direction, whereas $\mathbf{U}_N^{(y)}$ coincides with an electric dipole oriented along the same direction. Therefore, we call the beam $\mathbf{U}_M^{(x)}$ a "magnetic"-type and the $\mathbf{U}_N^{(y)}$ an "electric"-type linearly polarized beam.

The dependence of the multipole amplitudes C_{1n} and D_{1n} on the multipole order for different values of kz_0 are presented in Fig. 4. The maximum amplitude for a regular beam corresponds to a first order vector multipole; see Fig. 4(a). The dependence of the amplitudes of the first four multipole components C_{1n}, D_{1n} on the collimation distance kz_0 are depicted in Fig. 4(b). We note briefly that for $kz_0 > n$ the expansion coefficients of the irregular solution do not differ significantly from that of the regular solution and the multipole with highest amplitude is always $n \to \infty$ due to the presence of virtual sources in the model.

The beams $\mathbf{U}_M^{(y)}$, $\mathbf{U}_N^{(x)}$ are expanded in the same fashion. The decomposition of the function $\mathbf{L}_{0n} \times \mathbf{e}_x$ into VSHs can be written as

$$\mathbf{L}_{0n} \times \frac{2\mathbf{e}_x}{k} = \sum_{\nu=1}^{\infty} i \left[\frac{\mathbf{N}_{1,\nu}}{\nu(\nu+1)} + \mathbf{N}_{-1,\nu} \right] \delta_{\nu,n} - \left[\frac{\mathbf{M}_{1,\nu}}{\nu(\nu+1)} - \mathbf{M}_{-1,\nu} \right] \times \left[\frac{(\nu+1)\delta_{\nu,n+1}}{2\nu-1} \delta_{\nu,n+1} - \frac{\nu\delta_{\nu,n-1}}{2\nu+3} \right], \tag{22}$$

and the linearly polarized beams $\mathbf{U}_M^{(y)}$ and $\mathbf{U}_N^{(x)}$ are

$$\mathbf{U}_M^{(y)} = i \sum_{n=1}^{\infty} C_{1n}[\tilde{\mathbf{M}}_{1n} - \tilde{\mathbf{M}}_{-1n}] + D_{1n}[\tilde{\mathbf{N}}_{1n} + \tilde{\mathbf{N}}_{-1n}],$$
$$\mathbf{U}_N^{(x)} = i \sum_{n=1}^{\infty} C_{1n}[\tilde{\mathbf{N}}_{1n} - \tilde{\mathbf{N}}_{-1n}] + D_{1n}[\tilde{\mathbf{M}}_{1n} + \tilde{\mathbf{M}}_{-1n}]. \tag{23}$$

Besides the "pure" electric and magnetic linearly polarized beams, a variety of linear combinations are of interest. For example, we define two mixed-type beams which correspond to a tightly focused linearly polarized Gaussian beam [23]

$$\mathbf{U}^{(x)} = \frac{\mathbf{U}_M^{(x)} - i\mathbf{U}_N^{(x)}}{2},$$
$$\mathbf{U}^{(y)} = \frac{\mathbf{U}_M^{(y)} + i\mathbf{U}_N^{(y)}}{2}.$$

By putting Eqs. (20) and (23) into Eq. (24) the new expansion coefficients C'_{1n}, D'_{1n} are obtained as

$$C'_{1n} = \frac{C_{1n} + D_{1n}}{2} = D'_{1n}. \tag{24}$$

The comparison of the first five expansion coefficients C'_{1n} of the mixed-type beams is presented in Fig. 4(a).

A brief comparison of the expansion coefficients A_n and C_{1n}, D_{1n} reveals that under similar conditions, the amplitudes of the higher order multipoles are larger in the highly focused radially and azimuthally polarized beams than that of the linearly polarized beams. Indeed, the analysis of Eqs. (7) and (21) shows that $|A_n|/|C_{1n}| < |A_n|/|D_{1n}| = \sqrt{n(n+1)}$. Thus, the higher order multipoles are stronger in a radially polarized beam relative to those in a linearly polarized beam.

III. MULTIPOLE RESPONSE OF A SPHERICAL PARTICLE

Now we come to an application of the expansion into VSHs presented above. We develop an analytical Mie-like theory for highly focused CSBs which interact with a sphere situated in the origin. The derivations of the generalized Mie scattering theory, suitable for an arbitrary incoming electromagnetic field, follow the same steps as those described in classical textbooks dealing with the diffraction of a monochromatic plane wave of angular frequency ω by a homogeneous sphere with a radius R_{sp} and a complex refractive index n_{sp} embedded in a homogeneous nonabsorbing medium with refractive index n_m. In this theory, the incoming (index "inc") and scattered (index "sca") electric fields are expanded into normalized VSHs $\mathbf{M}_{mn}$, $\mathbf{N}_{mn}$ (see Refs. [10,24,28,33]):

$$\mathbf{E}_{\text{inc}} = \sum_{n=1}^{\infty} \sum_{m=-n}^{n} \left[A_{mn} \tilde{\mathbf{M}}_{mn}^{(1)} + B_{mn} \tilde{\mathbf{N}}_{mn}^{(1)} \right],$$
$$\mathbf{E}_{\text{sca}} = \sum_{n=1}^{\infty} \sum_{m=-n}^{n} \left[\alpha_n A_{mn} \tilde{\mathbf{M}}_{mn}^{(3)} + \beta_n B_{mn} \tilde{\mathbf{N}}_{mn}^{(3)} \right], \tag{25}$$

where the indices (1) and (3) denote regular and irregular VSHs, respectively. α_n, β_n are the classical Mie scattering coefficients, which can be associated with the natural modes of the sphere [34]. The amount of power dissipated by scattering, absorption (index "abs") and extinction (scattering plus absorption, index "ext") is obtained by the integration of the Poynting vectors flux over a sphere enclosing the particle. The dissipated energy rates are then expressed by [24,28,33]

$$W_{\mathrm{ext}} = \frac{1}{2k^2}\sqrt{\frac{\epsilon}{\mu}}\sum_{n=1}^{\infty}\sum_{m=-n}^{n}\mathrm{Re}(\alpha_n)|A_{mn}|^2 + \mathrm{Re}(\beta_n)|B_{mn}|^2,$$
$$W_{\mathrm{sca}} = \frac{1}{2k^2}\sqrt{\frac{\epsilon}{\mu}}\sum_{n=1}^{\infty}\sum_{m=-n}^{n}|\alpha_n|^2|A_{mn}|^2 + |\beta_n|^2|B_{mn}|^2, \quad (26)$$
$$W_{\mathrm{abs}} = W_{\mathrm{ext}} - W_{\mathrm{sca}}.$$

To characterize the interaction between beam and particle, we introduce efficiency factors $Q_{\mathrm{sca}} = W_{\mathrm{sca}}/W_{\mathrm{beam}}$ and $Q_{\mathrm{abs}} = W_{\mathrm{abs}}/W_{\mathrm{beam}}$.

In an experimental situation, usually the transmitted or the reflected light is detected in a limited solid angle, so we consider the energy scattered into the forward and backward hemisphere by introducing the transmission T and reflection R, which we define as

$$R = \frac{W_{\mathrm{sca}}(\pi/2,\pi)}{W_{\mathrm{beam}}}, \quad T = 1 - R - Q_{\mathrm{abs}}. \quad (27)$$

Next, the detectors usually do not collect the power from the whole hemisphere, but from a given solid angle defined by their numerical aperture $\mathrm{NA} = \sin\theta_a$. Therefore, we will briefly also consider the fraction of power scattered forwards $Q^f_{\mathrm{sca}}(\theta_a) = W_{\mathrm{sca}}(0,\theta_a)/W_{\mathrm{beam}}$ and backwards $Q^b_{\mathrm{sca}}(\theta_a) = W_{\mathrm{sca}}(\pi-\theta_a,\pi)/W_{\mathrm{beam}}$ with $W_{\mathrm{sca}}(\theta_1,\theta_2)$ defined as

$$W_{\mathrm{sca}}(\theta_1,\theta_2) = \frac{1}{2k^2}\sqrt{\frac{\epsilon}{\mu}}\sum_{\nu_1,\nu_2=1}^{\infty}\sum_{\mu=-\min(\nu_1,\nu_2)}^{\max(\nu_1,\nu_2)}\gamma_{\mu\nu_1}\gamma_{\mu\nu_2}\mathrm{Re}\{i^{\nu_2-\nu_1}[(\alpha_{\nu_1}A_{\mu\nu_1}\alpha^*_{\nu_2}A^*_{\mu\nu_2} + \beta_{\nu_1}B_{\mu\nu_1}\beta^*_{\nu_2}B^*_{\mu\nu_2})\Delta^{\mu}_{\nu_1\nu_2}(\theta_1,\theta_2)$$
$$+ (\alpha_{\nu_1}A_{\mu\nu_1}\beta^*_{\nu_2}B^*_{\mu\nu_2} + \beta_{\nu_1}B_{\mu\nu_1}\alpha^*_{\nu_2}A^*_{\mu\nu_2})\Sigma^{\mu}_{\nu_1\nu_2}(\theta_1,\theta_2)]\}, \quad (28)$$

where the first term ("dot" term) describes an interference between two electric (magnetic) multipoles and the second term ("cross" term) interference between an electric and a magnetic multipole. For the sake of the brevity we redirect readers to [35] for the exact expressions of $\Delta^{\mu}_{\nu_1\nu_2}(\theta_1,\theta_2)$ and $\Sigma^{\mu}_{\nu_1\nu_2}(\theta_1,\theta_2)$.

Before we proceed to the numerical examples, we will briefly discuss the differences in the scattering of the regular and irregular beams. The presence of virtual sources in the model gets important in the scattering process, as they give rise to infinitely high amplitudes of the higher order multipoles when $kz_0 < n$. As long as the scattering coefficients α_n, β_n vanish at least one order of magnitude faster than the expansion coefficients A_{0n}, C_{1n}, and D_{1n}, and the ratio R_{sp}/z_0 between the particle size R_{sp} and the radius z_0 of the virtual sources in the focal plane is smaller than unity, an irregular solution can be used along with a regular one without any restrictions. However, another problem arises for the regular solution. For infinitely small beam widths, it represents a standing spherical dipole wave, so the beam power vanishes [23] and the absorption Q_{abs} and scattering Q_{sca} become infinite in (28).

As an example for our numerical simulations we choose a spherical gold ($\epsilon = -21.17 + 0.73i$, [36]) particle with a radius of $R_{sp} = 75$ nm at a wavelength of $\lambda = 780$ nm. For the size parameter $kR_{sp} = 0.60$ we have truncated the expression for the scattered field in Eq. (25) at $n = 6$ [28]. We start with the dependence of the absorbed and total scattered power on the Rayleigh length kz_0 for five different cases; see Fig. 5(a) and 5(b). We see that the azimuthally polarized beam $\mathbf{U}_M$ interacts much less with the particle than the other beams. This is no surprise, because the electric field of the azimuthally polarized beam vanishes in its center, where the particle is situated. Also, the radially polarized beam $\mathbf{U}_N$ is absorbed less than the two "pure"-type linearly polarized beams, if the diffraction distance is larger than $kz_0 = 4.08$; see Fig. 5(a)–5(c). Again this is due to vanishing transverse electric field components on the optical axis. However, for smaller values of the collimation distance and beam width a strong longitudinal field starts to build up in the focus of the beam resulting in a stronger coupling and absorption. Finally, the gold sphere absorbs the radially polarized radiation even more than that of the linearly polarized beams. From the two "pure"-type linearly polarized beams, the "magnetic" beam $\mathbf{U}^{(x)}_M$ starts to absorb less and less than the "electric" one $\mathbf{U}^{(x)}_N$, when the beam gets smaller.

In Fig. 5(c) the amount of scattered energy in the forward and backward hemispheres is depicted. As one can see, for radially and azimuthally polarized beams slightly more light is scattered into the forward than into the backward direction. For linearly polarized beams, the opposite holds true. We note that the difference in the forward and backward scattered energies is larger for linearly polarized beams than for radially and azimuthally polarized ones. A particularly interesting situation is observed, when the values of kz_0 are between 2 and 4. Then the radially polarized beam is scattered more than the linearly polarized light in forward direction, but less in backward direction. In general, this observation holds true for small particles with stronger dipolar than quadrupolar responses or for highly focused CSBs.

Next, we model an experimental situation, where the scattered light is collected by a finite aperture detector. For small numerical apertures, the amount of scattered energy collected by a detector decreases faster for radially polarized light than for linearly polarized light. For angles $\theta_a < 45^\circ$, the radially polarized beam is scattered less than a linearly polarized beam; see Fig. 5(d).

The scattering and extinction efficiencies Q_{sca} and Q_{ext} approach values larger than unity, if the beam diameter is

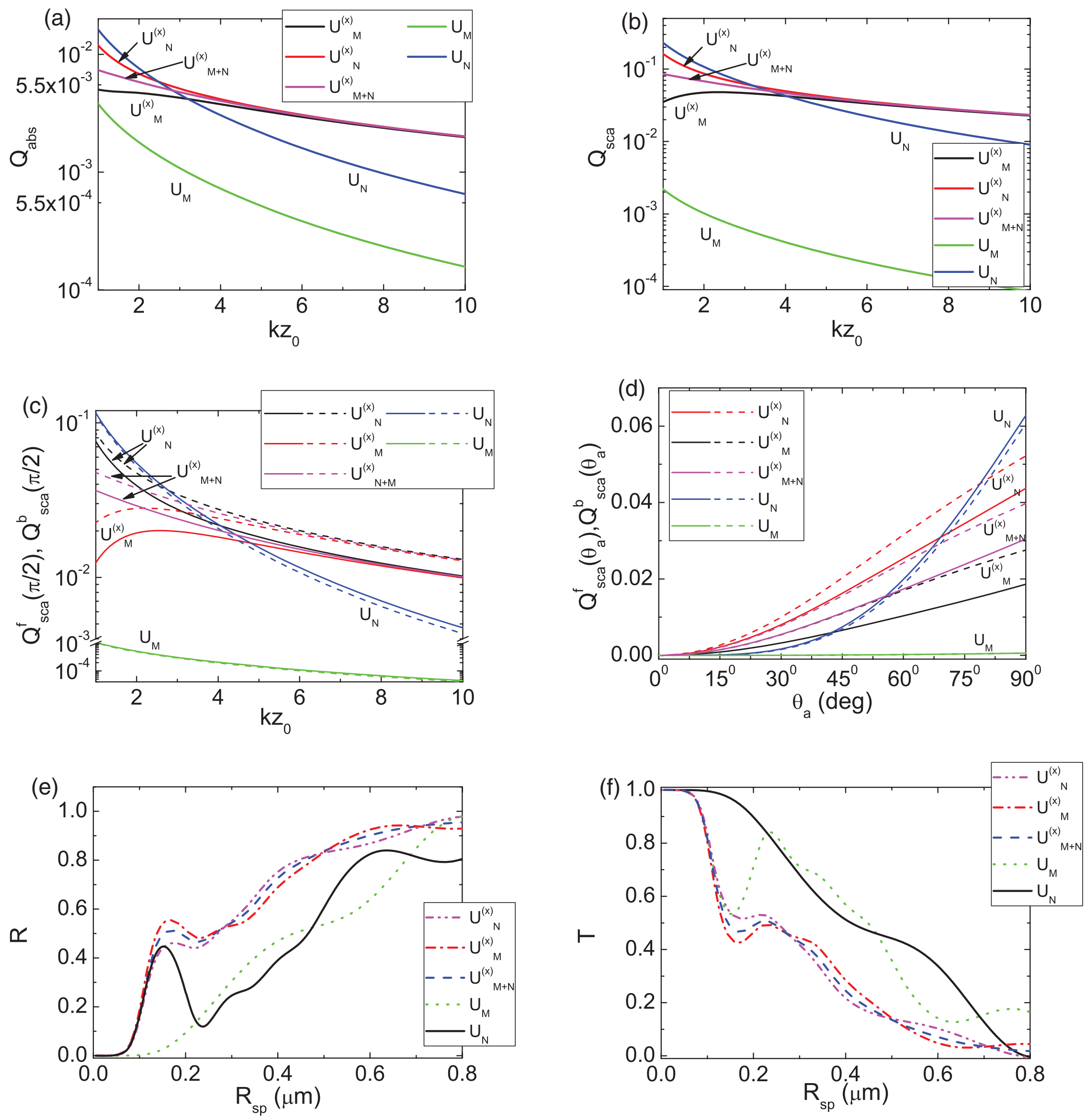

FIG. 5. (Color online) Dependence of the (a) absorbed, (b) total, and (c) forward and backward scattered energy on the collimation distance kz_0. The radius of the spherical gold particle under consideration is $R_{sp} = 75$ nm; the wavelength is $\lambda = 780$ nm. (d) Dependence of the forward and backward scattered energy on the numerical aperture angle θ_a for a ratio $w_0/\lambda = 0.3$ ($kz_0 = 0.18\pi^2$). Dependence of (e) the reflection R and (f) transmission T on the particle radius R_{sp} at $w_0/\lambda = 0.4$. The radially polarized beam is depicted in blue, the azimuthally polarized beam in green, and the linearly polarized beams $U_M^{(x)}$ and $U_N^{(x)}$ in black and red, correspondingly. The dashed line in panels c, d, e, and f corresponds to backward scattering, the solid line to forward scattering. The particle is centered on the optical axis in the focal plane.

smaller or comparable to the diameter of the particle. This accounts to the well-known fact that the extinction theorem is valid only for plane waves (see Refs. [15,37,38] for a detailed discussion). Therefore, we also investigate how the transmission and reflection (27) depend on the particle diameter. The dependencies for a particular collimation distance of $w_0/\lambda = 0.4$ at $\lambda = 780$ nm on the particle radius R_{sp} are presented in Figs. 5(e) and 5(f). It can be seen that the azimuthally polarized light is reflected less than all other polarizations until the radius of the particle reaches $R_{sp} \approx 230$ nm, when the magnetic response of the particle starts to dominate over the electric. The magnetic response of the particle is higher for a radius up to $R_{sp} \approx 460$ nm. The first maximum in the reflection of the radially polarized beam corresponds to the first electric dipole resonance at $R_{sp} \approx 150$ nm. The electric response of the sphere is minimal at $R_{sp} \approx 250$ nm. The linearly polarized beams are reflected more than the radially and azimuthally polarized beams, with the beam of the "magnetic" type $\mathbf{E}_M^{(x)}$ repeating the pattern of the azimuthally polarized beam and the beam of the "electric" type $\mathbf{E}_N^{(x)}$ following the trend of the radially polarized beam. The multipole responses are averaged in the "mixed"-type linearly polarized beams, which can be seen in the rather smooth corresponding curve. The scattering directivity is investigated further in Fig. 5(e). We

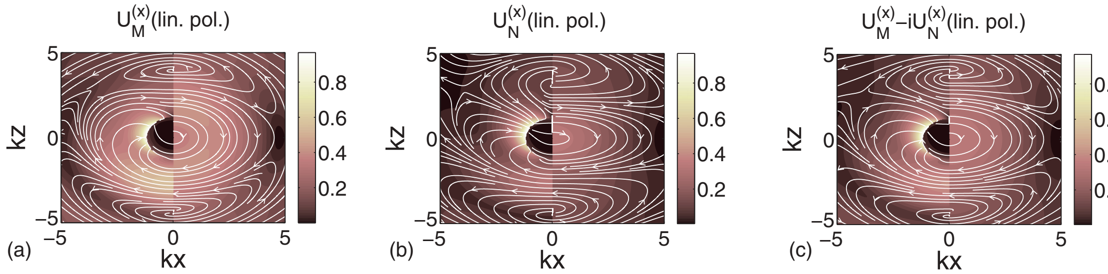

FIG. 6. (Color online) Modulus of the total (left side) and incident (right side) fields for the linearly polarized CSBs scattered on a gold sphere. The radius of the sphere is $R_{sp} = 75$ nm, the wavelength is $\lambda = 780$ nm and $kz_0 = 1.5$. The white arrows depict the direction of the electric vector **E**.

see that a polarization dependent scattering directivity is a typical property of a small particle with a high electric dipole response. It is clearly demonstrated that the optical response critically depends on the type of the impinging beam.

We end this section by showing the absolute value of the electric field distribution in the longitudinal plane (x,z) for one particular case (see Figs. 2 and 6). The left-hand side of the pictures show the total electric field with the particle being located at the center. The right-hand side of the pictures present the electric field of the incident beam without a particle being present. The scattering patterns of the azimuthally and radially polarized beams together with their linearly polarized TEM constituents are shown in Fig. 2. The scattering patterns for three different linearly polarized CSBs are demonstrated in Fig. 6.

IV. CONCLUSION

In conclusion, we have adopted the regular and irregular scalar complex source beam model and developed an analytical expansion of radially, azimuthally and linearly polarized vector CSBs into VSHs. Along with the highly focused radially and azimuthally polarized beams we considered also an analytical expansions of their linearly polarized constituents (beams after interaction with a nonparaxial linear polarizer). The differences between regular and irregular vector beams are diminishing as long as the beam waist and collimation distance remains large. When the beam waist reaches the size of the collimation distance, higher order multipoles dominate in the expansion of regular highly focused radially and azimuthally polarized beams compared to the expansion of linearly polarized beams.

An example of the Mie scattering of the considered fields on a small gold particle was investigated in detail. As a rule, the linearly and radially or azimuthally polarized beams have different scattering directivity. The linearly polarized beams scatter more into backward direction and the radially or azimuthally polarized ones more into forward direction. For small particles, radially polarized light usually scatters less than linearly polarized light under the same conditions.

ACKNOWLEDGMENTS

Sergejus Orlovas acknowledges the Humboldt Foundation and the Max Planck Society. Ulf Peschel acknowledges the support by the DFG funded Erlangen Cluster of Excellence "Engineering of Advanced Materials (EAM)."

[1] P. Zijlstra and M. Orrit, Rep. Prog. Phys. **74**, 106401 (2011).

[2] J. Seelig, K. Leslie, A. Renn, S. Kühn, V. Jacobsen, M. van de Corput, C. Wyman, and V. Sandoghdar, Nano Lett. **7**, 685 (2007).

[3] S. Kühn, U. Håkanson, L. Rogobete, and V. Sandoghdar, Phys. Rev. Lett. **97**, 017402 (2006).

[4] P. Banzer, U. Peschel, S. Quabis, and G. Leuchs, Opt. Express **18**, 10905 (2010).

[5] S. V. Boriskina and B. M. Reinhard, Nanoscale **4**, 76 (2012).

[6] E. Prodan, C. Radloff, N. J. Halas, and P. Nordlander, Science **302**, 419 (2003).

[7] S. N. Sheikholeslami, A. Garcia-Etxarri, and J. A. Dionne, Nano Lett. **11**, 3927 (2011).

[8] N. A. Mirin, K. Bao, and P. Nordlander, J. Phys. Chem. A **113**, 4028 (2009).

[9] M. Frimmer, T. Coenen, and A. F. Koenderink [http://arxiv.org/abs/1109.5407].

[10] G. Mie, Ann. Phys. **25**, 377 (1908).

[11] W.-C. Tsai and R. J. Pogorzelski, J. Opt. Soc. Am. **65**, 1457 (1975).

[12] W. G. Tam, Appl. Opt. **16**, 2016 (1977).

[13] J. S. Kim and S. S. Lee, J. Opt. Soc. Am. **73**, 303 (1983).

[14] G. Gouesbet, B. Maheu, and G. Grehan, J. Opt. Soc. Am. A **5**, 1427 (1988).

[15] J. A. Lock, J. Opt. Soc. Am. A **12**, 929 (1995).

[16] S. Quabis, R. Dorn, M. Eberler, O. Glöckl, and G. Leuchs, Opt. Commun. **179**, 1 (2000).

[17] K. S. Youngworth and T. G. Brown, Opt. Express **7**, 77 (2000).

[18] R. Dorn, S. Quabis, and G. Leuchs, Phys. Rev. Lett. **91**, 233901 (2003).

[19] T. Züchner, A. V. Failla, A. Hartschuh, and A. J. Meixner, J. Microsc. **229**, 337 (2008).

[20] N. M. Mojarad, V. Sandoghadar, and M. Agio, J. Opt. Soc. Am. B **25**, 651 (2008).

[21] N. M. Mojarad and M. Agio, Opt. Express **17**, 117 (2009).

[22] A. Wunsche, J. Opt. Soc. Am. A **5**, 765 (1992).

[23] S. Orlov and U. Peschel, Phys. Rev. A **82**, 063820 (2010)
[24] J. Stratton, *Electromagnetic Theory* (McGraw-Hill, New York, 1940).
[25] V. A. Markel, V. N. Pustovit, S. V. Karpov, A. V. Obuschenko, V. S. Gerasimov, and I. L. Isaev, Phys. Rev. B **70**, 054202 (2004).
[26] J. Petschulat, J. Yang, C. Menzel, C. Rockstuhl, A. Chipouline, P. Lalanne, A. Tennermann, F. Lederer, and T. Pertsch, Opt. Express **18**, 14454 (2010).
[27] S. Mühlig, C. Menzel, C. Rockstuhl, and F. Lederer, Metamaterials **5**, 64 (2011).
[28] L. Tsang, J. A. Kong, and K.-H. Ding, *Scattering of Eectromagnetic Waves* (John Wiley, New York, 2000).
[29] G. Gouesbet, Opt. Commun. **283**, 517 (2010).
[30] T. X. Hoang, X. Chen, and C. J. R. Sheppard, J. Opt. Soc. Am. A **29**, 32 (2012).
[31] Y. Fainman and J. Shamir, Appl. Opt. **23**, 3188 (1984).
[32] A. Aiello, C. Marquardt, and G. Leuchs, Opt. Lett. **34**, 3160 (2009).
[33] G. Gouesbet and G. Grehan, *Generalized Lorenz-Mie Theories* (Springer-Verlag, New York, 2011).
[34] R. Fuchs and K. L. Kliewer, J. Opt. Soc. Am. **58**, 319 (1968).
[35] J. Y. Son, W. M. Farmer, T. V. Giel Jr., Appl. Opt. **25**, 4332 (1986).
[36] M. J. Weber, *Handbook of Optical Materials* (CRC Press, Boca Raton, FL, 2003).
[37] J. A. Lock, J. T. Hodges, and G. Gouesbet, J. Opt. Soc. Am. A **12**, 2708 (1995).
[38] G. Gouesbet *et al.*, Opt. Commun. **125**, 137 (1996).